Chemical Engineering Journal 520 (2025) 166042

Contents lists available at ScienceDirect

Chemical Engineering Journal

journal homepage: www.elsevier.com/locate/cej

# Competitive $Li^+$ coordination in gel electrolyte enhances $Zn^{2+}$ kinetics and interfacial stability for low-temperature Zn-ion batteries

Mengfan Zhao [a,1], Bo Zhang [a,1], Xiang Bai [b], Jiahui Zhang [b], Xinyue Chang [c], Lifeng Hou [a,*], Hao Huang [a], Shi Wang [d,e,**], Zhong Jin [f,*], Qian Wang [a,g,***]

[a] College of Materials Science and Engineering, Taiyuan University of Technology, Taiyuan 030024, Shanxi, China
[b] Shanxi Energy Internet Research Institute, Taiyuan 030024, Shanxi, China
[c] Energy Internet Key Laboratory of Shanxi Province, Taiyuan 030024, Shanxi, China
[d] State Key Laboratory of Organic Electronics & Information Displays (SKLOEID), Institute of Advanced Materials (IAM), Nanjing University of Posts & Telecommunications, Nanjing 210023, China
[e] Key Laboratory of Functional Molecular Solids, Ministry of Education, Anhui Engineering Research Center of Carbon Neutrality, College of Chemistry and Materials Science, Anhui Normal University, Wuhu 241000, China
[f] State Key Laboratory of Coordination Chemistry, MOE Key Laboratory of Mesoscopic Chemistry, MOE Key Laboratory of High Performance Polymer Materials and Technology, Jiangsu Key Laboratory of Advanced Organic Materials, School of Chemistry & Chemical Engineering, Nanjing University, Nanjing 210023, China
[g] Guangdong Sirui Optics Co., Ltd, Zhongshan 523511, Guangdong, China

ARTICLE INFO

*Keywords:*
Zn metal anode
Zn-ion batteries
Gel electrolyte
$Zn^{2+}$-dipole
Interface

ABSTRACT

Gel electrolytes are garnering increased attention for rechargeable Zn-ion batteries (ZIBs) due to their high safety, excellent plasticity and high ionic conductivity. However, huge kinetic barriers and unstable solid electrolyte interface (SEI) film at low temperature limit their further application. Herein, we propose a $Li^+$ competitive coordination strategy in the polyacrylamide-based hydrogel framework cross-linked with polyethylene glycol (PEG), which synergistically addresses both bulk electrolyte dynamics and interfacial stability. Here, $Li^+$ can preferentially interact with polymer chains, weakening the $Zn^{2+}$-dipole interaction, thereby facilitating the $Zn^{2+}$ transport kinetics and de-solvation in gel electrolytes. At the same time, $Li^+$ can assemble into loosely bound solvation clusters surrounding the $Zn^{2+}$ solvation sheath, which not only immobilizes active $H_2O$ molecules, suppressing associated side reactions, but also preferentially reduce and form a Li—Zn hybrid and F-rich SEI layer on the Zn metal surface, significantly improving interface stability and promoting $Zn^{2+}$ migration through the SEI. Thus, the diffusion coefficient and ion transference number are significantly improved, while the $Zn^{2+}$ de-solvation energy down from 55 to 23 kJ $mol^{-1}$. As expected, the symmetrical cells can run stably over 6500 h at −20 °C, and full cells also deliver a high discharge capacity of 330 mAh $g^{-1}$ and high capacity retention after 700 cycles. This work offers a basic reference for designing gel electrolytes towards low-temperature ZIBs.

## 1. Introduction

Aqueous zinc-ion batteries have become a research hotspot in the field of energy storage due to their abundant resources, low cost and high safety, and are considered a potential alternative to lithium-ion batteries (LIBs). [1,2] However, in a typical aqueous electrolyte system, Zn metal anode often faces serious challenges, such as: hydrogen evolution reaction, surface corrosion, and dendrite growth due to the high chemical reactivity of $H_2O$, severely hindering the commercialization of ZIBs. [3,4]

Compared to aqueous electrolytes, the polymer chains in gel electrolytes are rich in hydrophilic groups (such as -OH and -$NH_2$), which

* Corresponding authors.
** Correspondence to: S. Wang, State Key Laboratory of Organic Electronics & Information Displays (SKLOEID), Institute of Advanced Materials (IAM), Nanjing University of Posts & Telecommunications, Nanjing 210023, China.
*** Correspondence to: Q. Wang, College of Materials Science and Engineering, Taiyuan University of Technology, Taiyuan 030024, Shanxi, China.
*E-mail addresses:* houlifeng@tyut.edu.cn (L. Hou), iamshiwang@njupt.edu.cn (S. Wang), zhongjin@nju.edu.cn (Z. Jin), qianwang0825@pku.edu.cn (Q. Wang).
[1] The authors contributed equally to this work.

https://doi.org/10.1016/j.cej.2025.166042
Received 7 May 2025; Received in revised form 26 June 2025; Accepted 14 July 2025
Available online 15 July 2025

can form strong hydrogen bonds with $H_2O$ molecules, effectively disrupting the original hydrogen bond network between $H_2O$ molecules, thereby significantly reducing its reactivity and effectively suppressing side reactions. [5,6] However, gel electrolytes still face huge challenges in practical applications, such as: poor ionic conductivity, low mechanical strength, and poor interface stability, [7–9] which lead to large kinetic barriers and unstable solid electrolyte interphase (SEI) films, especially at low-temperature environments. [10]

To address these challenges, many efforts have been devoted, such as: designing new gel electrolyte materials, nano-porous structure engineering, introducing conductive additives or cryoprotectants, regulating the hydrogen bonding network structure of the electrolyte, etc. [11–13] Its main purpose is to optimize the $Zn^{2+}$ channels to shorten the ion conduction pathway in gel electrolyte, so as to ensure rapid $Zn^{2+}$ transport at low temperatures. [14] However, every coin has two sides. Constructing $Zn^{2+}$ channels in gel electrolytes usually reduces ionic selectivity due to facilitated $H_3O^+$ conduction, resulting in high voltage hysteresis and interfacial resistance, and even severe $Zn^{2+}/H^+$ co-insertion at the cathode. [15] On the other hand, $H_2O$ molecules can form a hydration layer around the polymer chains, which functions as a lubricant, allowing solvated $Zn^{2+}$ to diffuse along it. [16] Based on this $Zn^{2+}$ transport mechanism, the following thoughts involuntarily arise: can we reduce the affinity between $Zn^{2+}$ and polymer chains, while optimizing the clusters around solvated $Zn^{2+}$, thereby ensuring fast $Zn^{2+}$ transport kinetics at low temperatures and forming stable SEI film.

Herein, as a conceptual validation, we synergistically weaken the $Zn^{2+}$-dipole and optimize the clusters around solvated $Zn^{2+}$ via a $Li^+$ competitive coordination strategy in gel electrolytes. [17] Here, $Li^+$ can compete with $Zn^{2+}$ and preferentially interact with polymer chains, weakening the $Zn^{2+}$-dipole interaction without altering the $Zn^{2+}$ solvation structure, thereby facilitating the $Zn^{2+}$ transport kinetics and desolvation at low temperatures. At the same time, $Li^+$ can assemble into loosely bound solvation clusters surrounding the $Zn^{2+}$ solvation sheath, which not only immobilizes active $H_2O$ molecules and lowers the freezing point of electrolyte, suppressing associated side reactions, but also functions as a lubricant, promoting the rapid diffusion of solvated $Zn^{2+}$ through electrostatic repulsion. Furthermore, a Li—Zn hybrid and F-rich SEI layer on the Zn metal surface can be formed during electrochemical cycling, significantly improving interface stability and promoting $Zn^{2+}$ migration through the SEI.

## 2. Results and discussion

### 2.1. Design concept and $Zn^{2+}$ diffusion mechanism

According to the latest reports, for a typical gel electrolyte in ZIBs, the monomer with a large number of hydrophilic groups is usually used to increase the hydrophilicity of polymer chains, so that $H_2O$ molecules can be fixed on the polymer chain as much as possible, reducing the content of free $H_2O$ molecules, thus broadening the voltage window and inhibiting side reactions. [18] This leads to $Zn^{2+}$ transportation mainly through structural diffusion, also known as Grotthuss diffusion, which involves multiple mechanisms. [19] 1) For hydrophilic groups, $H_2O$ molecules form a hydration layer around the polymer chains, severing as a lubricant to assist solvated $Zn^{2+}$ diffusion; 2) For polyanionic gel electrolytes, $Zn^{2+}$ transportation mainly through electrostatic interaction; 3) For polycationic gel electrolytes, $Zn^{2+}$ moves along the anions anchored to the polymer frameworks. [20] Based on this, we proposed a $Li^+$ competitive coordination strategy in gel electrolytes to synergistically weaken the $Zn^{2+}$-dipole and optimize the clusters around solvated $Zn^{2+}$, thus improving $Zn^{2+}$ transportation and forming stable SEI film. In this study, the molecular weights of polyacrylamide (PAM) and polyethylene glycol (PEG) significantly influence the mechanical strength, ionic conductivity, and liquid absorption of the gel electrolyte. We selected high-molecular-weight PEG (20000) as the crosslinking agent and PAM as the hydrogel framework, and introduced LiCl salt to fabricate a hydrophilic gel electrolyte. By optimizing the reaction conditions, we enhanced the mechanical properties while balancing the ionic conductivity and other performance characteristics. It is worth noting that the amount of LiCl has a significant influence on the performance of the gel electrolyte. An appropriate amount of LiCl can enhance the ionic conductivity, porosity, and mechanical strength. However, an excessive amount of LiCl will lead to a decrease in ionic conductivity, pore blockage, and a reduction in mechanical properties. Therefore, optimizing the amount of LiCl is crucial for balancing the overall performance of the gel electrolyte. As shown in Fig. 1, after introducing LiCl salts into gel electrolytes, a distinctive $Li^+$ had been validated, which played multiple key roles. 1) Forming competitive coordination with $Zn^{2+}$ to weaken the $Zn^{2+}$-dipole interaction; 2) Assembling into loosely bound solvation clusters surrounding the $Zn^{2+}$ solvation sheath to ensure the rapid $Zn^{2+}$ diffusion; 3) Immobilizing active $H_2O$ molecules; 4) Forming a Li—Zn hybrid SEI layer during electrochemical cycling; 5) Promoting the aggregation of polymer chains, thereby improving their tensile strength. Based on the above characteristics, the gel electrolyte delivered a high mechanical toughness and rapid $Zn^{2+}$ transport kinetics, as well as de-solvation at low temperatures. Meanwhile, associated side reactions, such as: hydrogen evolution reaction (HER), surface corrosion, were significantly suppressed.

In the gel electrolyte of ZIBs, the existence form of $H_2O$ molecule is closely related to its hydrogen bond strength, which directly affects the ion conductivity and interface stability of the gel electrolyte. Specifically, network water (NW), that is, a continuous three-dimensional network structure formed by a large number of $H_2O$ molecules through strong hydrogen bonds (similar to liquid water). It is prone to causing side reactions, leading to Zn dendrite growth and interface instability. Intermediate water (IW), water molecules disturbed by salt ions (such as: $Zn^{2+}$, $Cl^-$) or other additives in the gel electrolyte can partially break the hydrogen bond network. Multimer water (MW), that is $H_2O$ molecules strongly adsorbed by anions or polymer chains form localized small clusters, exhibiting low reactivity. [21] Subsequently, the reactivity of $H_2O$ molecules and their hydrogen bonding network under the $Li^+$ competitive coordination strategy were analyzed in detail. In the full infrared spectrum, the O—H bond shows the most significant changes after the introduction of $Li^+$ (Fig. S1). As shown in Fig. 2a, after introducing $Li^+$ into the gel electrolyte, the stretching vibration of O—H bond in infrared spectrum (2900–3700 $cm^{-1}$) had undergone significant changes, which was closely related to the existence form of $H_2O$ molecules, NW, IW and MW. And the blue shift of O—H peak indicated that the number of strong hydrogen bonds in the gel electrolyte decreased, corresponding to a decrease of the content of NW. Furthermore, Raman spectroscopy was also used to analyze the changes in hydrogen bonds. [22] As shown in Fig. 2b, the peaks at 3240, 3410, and 3580 $cm^{-1}$ corresponding to strong hydrogen bonds, medium hydrogen bonds, and weak hydrogen bonds, respectively. [23] At the same time, the relative proportions of $H_2O$ molecules in various states can be quantified through peak area integration, which was shown in Fig. 2c. After introducing $Li^+$ into the gel electrolyte, the proportion of NW can be decreased from 26.6 % to 17.75 %, while the proportion of IW increased. These results indicated that the introduction of $Li^+$ can effectively weaken the hydrogen bonds between $H_2O$ molecules and reduce their reactivity.

Then, we started focusing on the coordination structure of zinc ions and their interactions with water molecules. After introducing $Li^+$ in gel electrolytes, a second platform appeared in the Fig. 2d, corresponding to the outer solvation cluster, which suggested that $Li^+$ can interact with polymer chains to form loose clusters, thus weakening the interaction between $Zn^{2+}$ and $H_2O$ molecules. Furthermore, we analyzed the details about the solvation structures by the radial distribution function (RDF). As shown in Fig. 2e, for the bare gel electrolyte without $Li^+$ doping, the average coordination numbers for $Zn^{2+}$ with $OTf^-$, $H_2O$, acrylamide, and polyethylene glycol were 0.60, 4.88, 0.04, and 0.04, respectively.

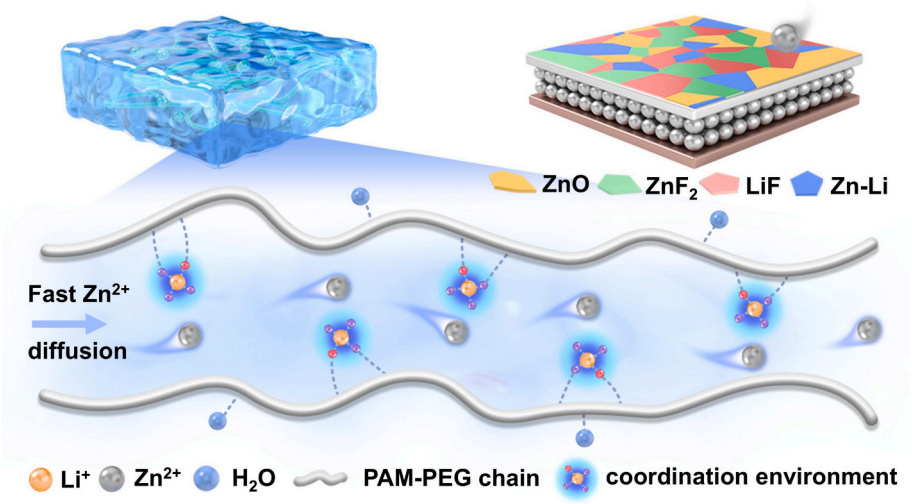


**Fig. 1.** Schematic diagram of zinc ion deposition and transportation in electrolyte.

However, after introducing $Li^+$ in gel electrolytes, the average coordination numbers for $Li^+$ with these components were 0.32, 4.13, 0.14 and 0.13 (Fig. 2f), suggesting that $Li^+$ can form competitive coordination with $Zn^{2+}$ and preferentially interact with polymer chains. The decrease in the average coordination number between $Zn^{2+}$ and polymer chains also confirms this conclusion (Fig. 2g). Meanwhile, doping $Li^+$ decreased the coordination number of $Zn^{2+}$-$H_2O$ from 4.88 to 4.77, further confirming that $Li^+$ can form loose clusters surrounding the $Zn^{2+}$ solvation sheath, thus weakening the interaction between $Zn^{2+}$ and $H_2O$ molecules, which was beneficial for the $Zn^{2+}$ diffusion and de-solvation. We have also examined the interactions of $Zn^{2+}$ and $Li^+$ ions with N and $Cl^-$ in both electrolyte systems (Fig. S2). We found that in both systems, one water molecule in the coordination environment of $Zn^{2+}$ ions was replaced by a $Cl^-$. This coordination change weakened the strong interactions between $Zn^{2+}$ ions and solvent molecules, thereby reducing the desolvation energy barrier and facilitating ion transport.

Furthermore, the coordination environment of $Zn^{2+}$ ions was investigated by molecular dynamics (MD) simulations. As shown in Fig. 2h and Fig. S3, the coordination structures of $Zn^{2+}$ in both systems were highly consistent, suggesting that $Li^+$ doping only weakened the $Zn^{2+}$-dipole interaction and did not change the solvation structure of $Zn^{2+}$ ions. Additionally, we carried out nuclear magnetic resonance (NMR) analysis of $^7Li$ on the gel electrolyte only with $Li^+$ and the gel electrolyte with $Li^+$ and $Zn^{2+}$ to explore the coordination environment of $Li^+$. As shown in Fig. 2i, $^7Li$ NMR spectra showed that there was no obvious shift, also suggesting that $Li^+$ can form competitive coordination with $Zn^{2+}$ and preferentially interact with polymer chains.

Meanwhile, we also evaluated the interactions between polymer chains and $H_2O$ molecules. As shown in Fig. 2j, the bond energies of $H_2O$ molecules with $H_2O$ molecules, polyacrylamide (PAM) and polyethylene glycol (PEG) were -0.33 eV, -0.54 eV and -0.63 eV, respectively, suggesting strong interaction between $H_2O$ molecules and polymer chains, which reduced the availability of free $H_2O$ molecules and consequently improved the structural integrity of gel electrolytes. The contact angle test can also confirm this conclusion (Fig. S4). Furthermore, the lowest unoccupied molecular orbital (LUMO) and the highest occupied molecular orbital (HOMO) of different salts were also calculated. Generally speaking, a smaller energy gap between HOMO and LUMO means higher conductivity and faster charge transfer rates. [24] As shown in Fig. 2k, the order of energy gaps was $Zn(OTf)_2$ < LiCl-$H_2O$ < LiCl < $ZnCl_2$ < $ZnCl_2$-$H_2O$, suggesting $Zn(OTf)_2$ and LiCl were easily decomposed, thus forming a Li—Zn hybrid and F-rich SEI layer on the Zn metal surface during electrochemical cycling. Such a SEI reduced the reactivity of Zn metal surface, meanwhile, the presence of $Li^+$ helped regulate the Zn deposition behavior and suppress dendrite formation, thereby significantly enhancing interfacial stability. Additionally, the F-rich SEI layer had excellent chemical stability and mechanical strength, ensuring high interface stability. Furthermore, we conducted in-situ EIS tests to analyze the interfacial stability. As shown in Fig. S5, for the bare gel electrolyte, the EIS exhibited very significant fluctuations, corresponding to unstable interface. However, after doping $Li^+$ into the electrolyte, it displayed an increasing trend, which can be attributed to the gradual formation of the SEI layer. Correspondingly, the DRT profiles can also confirm this conclusion (Fig. S6).

### 2.2. $Zn^{2+}$ diffusion and deposition behavior analysis

The $Zn^{2+}$ diffusion is directly related to the ionic conductivity of gel electrolytes, which can be determined through electrochemical impedance spectroscopy (EIS). [25] As shown in Fig. 3a, the ionic conductivity of the gel electrolyte after doping $Li^+$ was 11.67 mS $cm^{-1}$ at room temperature, which was far higher than that of bare gel electrolyte (7.03 mS $cm^{-1}$), showing fast $Zn^{2+}$ transport kinetics. The EIS tests also revealed that the gel electrolyte doped with $Li^+$ exhibited a lower interfacial impedance(Fig. S7), which further demonstrated its superior ion transport properties. Furthermore, mean square displacement (MSD) curves also confirmed that. As shown in Fig. 3b, the gel electrolyte after doping $Li^+$ demonstrated a higher $Zn^{2+}$ diffusion coefficient (200.82 $pm^2/ps$) than the bare gel electrolyte (104.40 $pm^2/ps$), which can be attributed to the introduction of $Li^+$ weakened the $Zn^{2+}$-dipole and optimized the clusters around solvated $Zn^{2+}$. Besides, transference number is also a crucial parameter for the $Zn^{2+}$ diffusion, and a high $Zn^{2+}$ transference number can inhibit the formation of space charge and form more stable SEI layer. As shown in Fig. 3c and Fig. S8, the $Zn^{2+}$ transference number of the gel electrolyte after doping $Li^+$ was 0.67, which was higher than that of the bare gel electrolyte (0.43), once again proving the positive role of $Li^+$. Rapid $Zn^{2+}$ transport kinetics can effectively reduce the concentration polarization and regulate ion diffusion, thereby suppressing dendritic Zn growth and achieving stable ZIBs. After that, we also tested the EIS of symmetric cells at different temperatures and calculated the activation energy ($E_a$). According to previous reports, $E_a$ reflects the difficulty of ion transport at the electrode/electrolyte interface, representing the energy required for ions to detach from the electrolyte body at the interface and enter the electrode surface. Therefore, it can also be referred to as: de-solvation energy. As shown in Fig. 3d and Fig. S9, compared with the bare gel electrolyte ($E_a$ = 55 kJ $mol^{-1}$), the gel electrolyte after doping $Li^+$ displayed a smaller de-solvation energy ($E_a$ = 23 kJ $mol^{-1}$), indicating that the $Li^+$

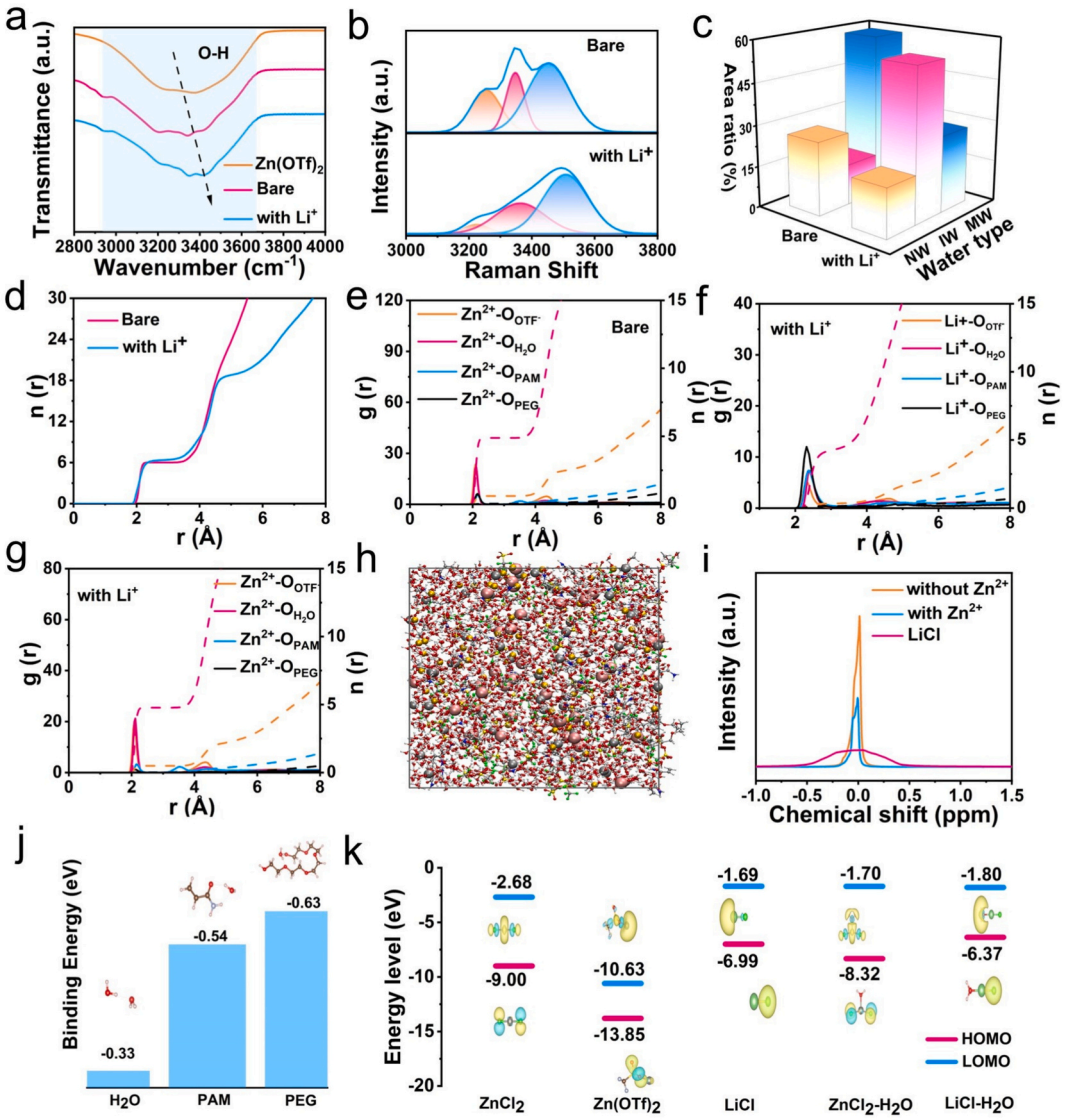


**Fig. 2.** Solvation structure and $Zn^{2+}$ diffusion mechanism. a) FT-IR spectra of $Zn(OTf)_2$, bare gel electrolyte and the gel electrolyte with $Li^+$ doping; b) Fitting Raman spectra of O—H stretching vibrations; c) Different types of water in the bare gel electrolyte and the gel electrolyte with $Li^+$ doping; d) Coordination number of total Zn—O pairs in the gel electrolyte; e&g) Radial distribution function and coordination number of Zn—O in the bare gel electrolyte and the gel electrolyte with $Li^+$ doping; f) Radial distribution function and coordination number of Li—O in the gel electrolyte with $Li^+$ doping; h) Simulated 3D snapshots in the gel electrolyte with $Li^+$ doping; i) $^7Li$ nuclear magnetic resonance (NMR) spectrum. j) Binding energies of $H_2O$-$H_2O$, $H_2O$-PAM, and $H_2O$-PEG. k) HOMO and LUMO energy levels.

competitive coordination strategy can promote the rapid $Zn^{2+}$ transport kinetics at the electrode/electrolyte interface, thereby ensuring stable run of ZIBs at low temperatures. Following closely, differential scanning calorimetry (DSC) curves showed the freezing point of the gel electrolyte was −23.1 °C (Fig. 3e). Low freezing point can be attributed to the abundant amide groups in PAM and the ether oxygen bonds in PEG, which effectively disrupted the hydrogen bonding network between $H_2O$ molecules. [26] And after introducing $Li^+$ into the gel electrolyte, the freezing point further dropped to −41.7 °C, indicating that the interaction between $Li^+$ and $H_2O$ molecules further suppresses the activity of $H_2O$, weakening the hydrogen bonds between $H_2O$ molecules, thereby resulting in a significant decrease in the freezing point of the gel electrolyte, which was crucial for enhancing the $Zn^{2+}$ diffusion behavior under low-temperature conditions. Even at low-temperature environments, the gel electrolyte also demonstrated rapid $Zn^{2+}$ diffusion and desolvation. At −20 °C, after introducing $Li^+$ into the gel electrolyte, it achieved a high ionic conductivity of 4.72 mS/cm (Fig. S10) and $Zn^{2+}$ transference number of 0.4 (Fig. S11). In contrast, the bare gel electrolyte struggled to facilitate effective $Zn^{2+}$ diffusion at low temperatures, with a $Zn^{2+}$ transference number of merely 0.1. Moreover, the gel electrolyte with $Li^+$ doping exhibited a relatively low activation energy of 16 kJ $mol^{-1}$ at low temperatures (Fig. S13), further confirming its rapid $Zn^{2+}$ diffusion and de-solvation. These outstanding properties lay a solid foundation for the efficient cycling of ZIBs at low-temperature application."

The electrochemical stability of different gel electrolytes was also measured by linear sweep voltammetry (LSV). As shown in Fig. S14, the electrochemical window was expanded after introducing $Li^+$ into the gel electrolyte, up to 2.6 V, which can match with common cathode materials. Meanwhile, stress-strain curves demonstrated that doping $Li^+$ into the gel electrolyte can promote the aggregation of polymer chains, thereby improving tensile strength (Fig. S15). Then, $Zn^{2+}$ nucleation and deposition behavior was further analyzed. As shown in Fig. 3f, after introducing $Li^+$ into the gel electrolyte, the nucleation overpotential increased from 5.83 mV to 12.31 mV, corresponding to a higher driving force for nucleation, which promoted dense Zn deposition during the subsequent growth process. At the same time, $Li^+$ can preferentially adsorb onto the electrode surface to promote uniform Zn deposition

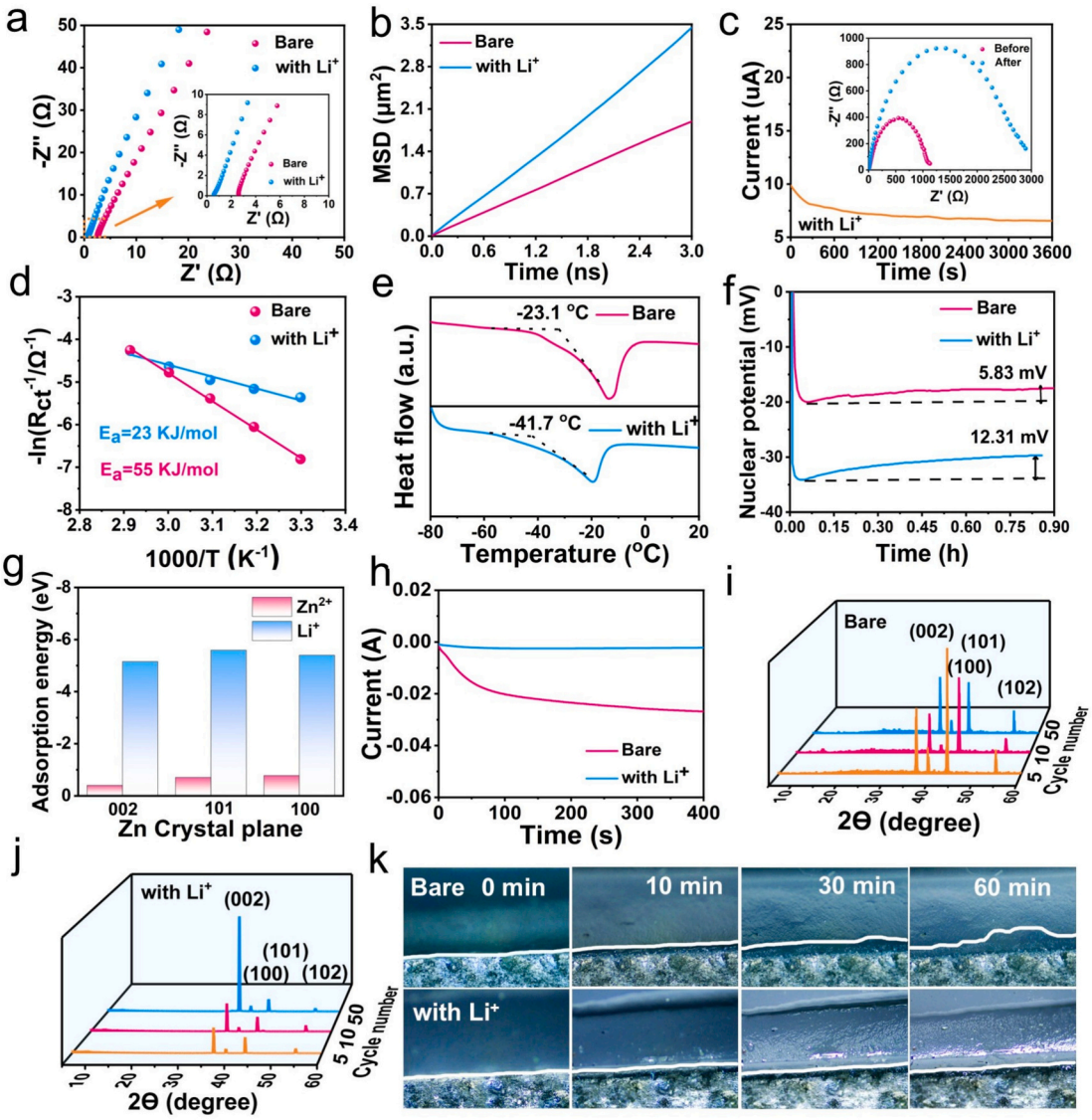


**Fig. 3.** $Zn^{2+}$ diffusion and deposition behavior analysis. a) Ionic conductivity of the gel electrolyte with or without $Li^+$ doping; b) Simulations of the $Zn^{2+}$ diffusion coefficient in the gel electrolyte with or without $Li^+$ doping via MSD analysis; c) $Zn^{2+}$ transference number of the gel electrolyte with $Li^+$ doping; d) Activation energy; e) DSC curves; f) Nucleation potentials at a current density of 0.2 mA $cm^{-2}$; g) Adsorption energy of $Zn^{2+}$ and $Li^+$ on different crystal planes; h) Chronoamperograms at an overpotential of −150 mV; (i&j) XRD of Zn metal anode after cycling in the gel electrolyte without (i) or with $Li^+$ doping (j); k) In situ optical images of Zn plating in different gel electrolyte systems.

based on electrostatic shielding mechanism (Fig. 3g). Specifically, after introducing $Li^+$ into the gel electrolyte, during the Zn deposition process, $Li^+$ will act like a hat to weaken the local electric field strength at the tip, forcing $Zn^{2+}$ to tend to deposit around the area covered by $Li^+$, rather than accelerating growth at the tip where the electric field is concentrated, thereby leading uniform Zn deposition. Furthermore, the AC impedance tests showed that the $Li^+$-doped gel electrolyte exhibited a more positive zero-charge potential and lower capacitance characteristics, indicating an optimized charge balance on the electrode surface, thus promoting uniform Zn deposition (Fig. S16). In addition, the chronoamperometry (CA) curves were also characterized to analyze the Zn nucleation and growth behavior. [27] As shown in Fig. 3h, when the polarization voltage was fixed at −150 mV, the response current continued to increase over 400 s in the bare gel electrolyte, corresponding to a random 2D $Zn^{2+}$ diffusion process, thereby leading to the formation of more electro-deposition sites and increased Zn deposition rate, which ultimately resulted in uncontrolled Zn dendrites. [28] In contrast, after introducing $Li^+$ into the gel electrolyte, continuous 3D $Zn^{2+}$ diffusion can be achieved, corresponding to the lateral and parallel Zn deposition. X-ray diffraction (XRD) measurements were also performed on the Zn metal anode after cycling. [19] As shown in Fig. 3i and Fig. 3j, for the bare gel electrolytes, the main growth direction of Zn metal was dominated by the Zn (101) crystalline plane, indicating irregular Zn deposition and dendritic Zn formation. However, with the introduction of $Li^+$, XRD patterns demonstrated a significant change, that is, Zn deposition mainly occurred along the Zn (002) direction, and as the number of cycles increased, the intensity of the Zn (002) plane significantly strengthened. Furthermore, according to the (002)/(100) peak intensity ratio during the cycling process, after doping $Li^+$ into the gel electrolyte, the intensity ratio of the (002)/(100) peak increased from 0.98 to 1.86 after 50 cycles, showing the Zn (002) plane was main Zn deposition direction (Fig. S17), which was consistent with the results of previous CA curves. Furthermore, an in situ optical device was carried out to observe the Zn deposition behavior, which was shown in Fig. 3k. For the aqueous electrolyte (Fig. S18), during the initial stages of Zn deposition, an uneven surface with irregular protrusions began to form,

and as deposition time increased, these protrusions grew further, triggering a self-amplification process that ultimately leaded to the formation of Zn dendrites. [29] However, after introducing $Li^+$ into the gel electrolyte, a dense and uniform Zn layer can be observed, maintaining a dendrite-free surface even after 60 min of Zn deposition. The above results indicated that doping $Li^+$ into the gel electrolyte can regulate the $Zn^{2+}$ diffusion and deposition behavior, achieving uniform Zn deposition.

### 2.3. Interface stability and electrochemical performance at room temperature

To investigate the effect of $Li^+$ doping on the interface stability of gel electrolytes, we first measured the hydrogen evolution potential of the gel electrolyte. As shown in Fig. S19, after introducing $Li^+$ into the gel electrolyte, the hydrogen evolution overpotential had undergone a significant negative shift, indicating inhibited hydrogen evolution reaction. [30] As well known, the hydrogen evolution reaction and corrosion reaction occur simultaneously. Subsequently, linear polarization tests were used to analyze the corrosion behavior. As shown in Fig. S20, after doping $Li^+$ into the gel electrolyte, the corrosion potential shifted positively from −14.7 mV to −5.1 mV, and the corrosion current decreased from 1.78 mA $cm^{-2}$ to 0.229 mA $cm^{-2}$, indicating improved interface stability. Furthermore, we also compared the surface morphology of Zn metal anode after cycling. As shown in Fig. S21, the Zn metal surface after cycling the bare gel electrolyte exhibited uneven surface morphology and obvious corrosion pits. By comparison, when using the gel electrolyte with $Li^+$ doping, the Zn electrode exhibited a relatively smooth surface morphology and there were no obvious by-products.

Then, we also conducted XPS analysis on the Zn metal anode after cycling to explore the SEI film. As shown in Fig. 4a, for the Zn metal anode cycling in the bare gel electrolyte, the peaks at 1022.5 eV and 1045.2 eV correspond to Zn 2p3/2 and Zn 2p1/2, respectively. [31] And in the F 1s spectrum (Fig. 4b), we distinctly observed signals belonging to $ZnF_2$ and C—F. However, after introducing $Li^+$ into the gel electrolyte, the peak of Zn 2p1/2 shifted significantly towards the direction of lower binding energy, indirectly explaining the formation of Li—Zn hybrid SEI layer. Meanwhile, the peak of $ZnF_2$ in the F 1s spectrum was stronger, and two distinct peaks corresponding to the LiF and Li—Zn were observed in the Li 1s XPS spectrum (Fig. 4c). These results confirmed that $Li^+$ can assemble into loosely bound solvation clusters surrounding the $Zn^{2+}$ solvation sheath, thereby deriving a Li—Zn hybrid and F-rich SEI layer on the Zn metal surface during electrochemical cycling, which significantly improved interface stability and promoted $Zn^{2+}$ migration through the SEI.

To investigate the impact of $Li^+$ doping in gel electrolytes on electrochemical performance, we assembled Zn || Zn symmetric cells. As shown in Fig. 4d, at room temperature and a current density of 0.2 mA $cm^{-2}$, the symmetric cells using the gel electrolyte with $Li^+$ doping can stably cycle for 1500 h, whereas the symmetric cells displayed obvious voltage fluctuation after 270 h in the bare gel electrolyte, which can be attributed to internal hydrogen evolution reactions and uncontrolled dendrite growth. Even at a high current density of 0.5 mA $cm^{-2}$, the Zn || Zn symmetric cells can also display a long cycling life (400 h) after doping $Li^+$ into the gel electrolyte (Fig. S22). Similarly, we also assembled Zn | Cu half cells to evaluate the coulombic efficiency (CE). As shown in Fig. 4e, the half cells in bare gel electrolyte failed after 500 cycles due to severe interfacial side reactions and dendritic growth, while the CE in the electrolyte with $Li^+$ doping can maintain stable over

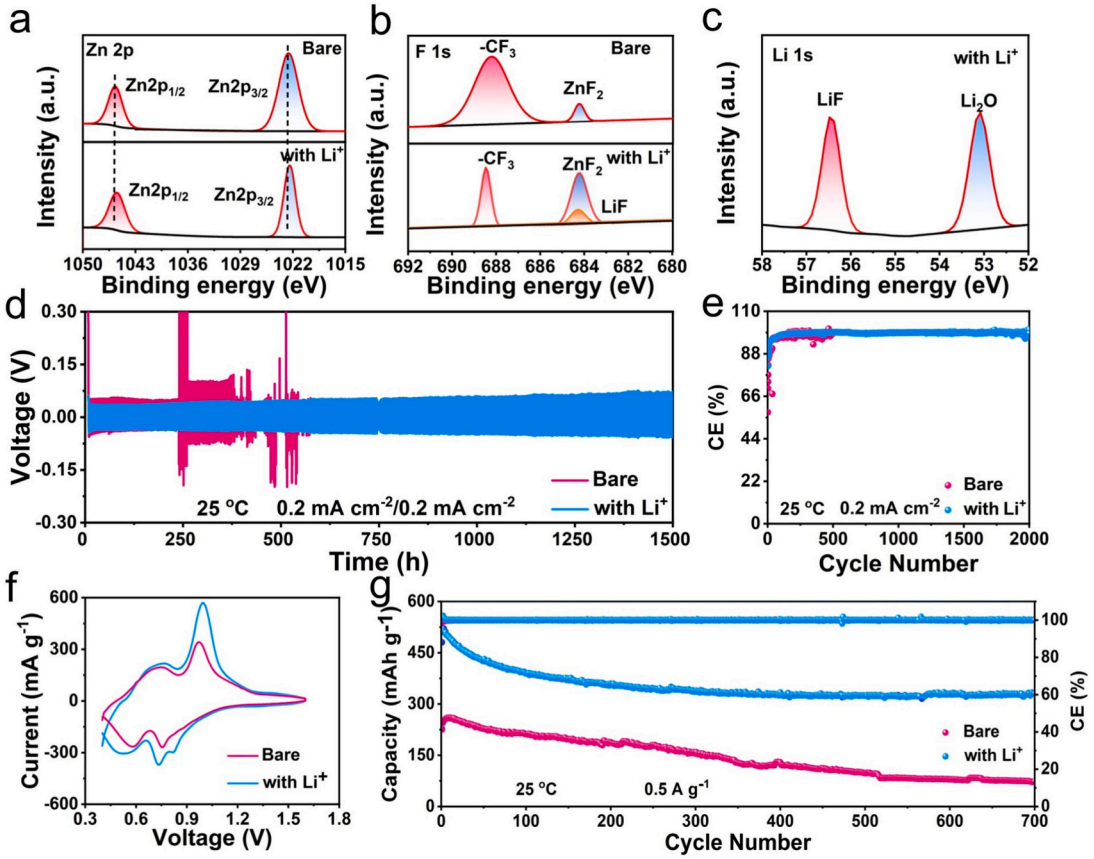


**Fig. 4.** Interface stability and electrochemical performance at room temperature. a-c) XPS spectra of Zn metal anode after 50 cycles, Zn 2p (a); F 1s (b); Li 1s (c). d) Long cycling stability of Zn || Zn symmetric cells at room temperature; e) Long cycling stability of Zn | Cu half cells; f) CV curves of full cells; g) Cycling performance of full cells at 0.5 A $g^{-1}$.

2000 cycles, showing high reversibility. Furthermore, we synthesized the NVO cathode based on previous reports, [32] XRD and SEM confirmed its successful synthesis (Fig. S23 and S24). We conducted cyclic voltammetry (CV) tests (Fig. 4f), at a scan rate of 0.1 mV/s, the cells exhibited similar redox peaks, but the cells using the gel electrolytes with $Li^+$ doping demonstrated superior reversibility and higher peak currents. [33,34] To further confirm the reversibility of the full cells, we conducted a detailed comparison analysis of the dQ/dV curves over multiple charge-discharge cycles. As shown in Fig. S25, the dQ/dV curves highly overlapped in subsequent cycles, indicating that the electrochemical reaction process of the full cells was highly reversible without significant side reactions or structural degradation. For the cycling stability, which was shown in Fig. 4g. At room temperature and a current density of 0.5 A $g^{-1}$, the cells using the gel electrolyte with $Li^+$ doping exhibited a high discharge capacity of 510 mAh $g^{-1}$ and high capacity retention after 700 cycles. In contrast, the discharge capacity using bare gel electrolyte failed rapidly, highlighting the significant advantage of $Li^+$-doping in enhancing battery performance.

### 2.4. Application at low temperature

To explore the practical application of the $Li^+$ competitive coordination strategy in gel electrolyte for ZIBs at low temperature, we firstly evaluated the rate performance of symmetric cells at −20 °C under a current density range of 0.05 to 0.5 mA $cm^{-2}$. [35] As shown in Fig. 5a, after doping $Li^+$ into the gel electrolyte, the symmetric cells exhibited smaller overpotentials and stable cycling performance. Besides, we investigated the cycling stability of symmetric cells. As shown in Fig. 5b, at −20 °C, the cells using the bare gel electrolyte experienced failure after only 220 h and showed significant voltage fluctuations. In contrast, the cells cycling in the electrolyte with $Li^+$ doping demonstrated ultra-long cycling stability (>6500 h) and stable voltage polarization. And for full cells, the cells using the electrolyte with $Li^+$ doping can display a high discharge capacity and long cycling performance (Fig. 5c and Fig. 5d), showing excellent application prospects. Even if the temperature dropped to −40 °C, the bare gel electrolyte would freeze, rendering the cell inoperable. However, when introducing $Li^+$ into the gel electrolyte, the freezing point of gel electrolyte was significantly reduced, enabling the cells to run stably for over 4500 h at −40 °C (Fig. 5e). And full cells also can maintain a high discharge capacity after 800 cycles (Fig. 5f). These results indicated that doping $Li^+$ into gel electrolyte can significantly enhance the electrochemical performance under low-temperature conditions.

## 3. Conclusion

In summary, this work developed a $Li^+$ competitive coordination strategy in gel electrolytes to synergistically weaken the $Zn^{2+}$-dipole and optimize the clusters around solvated $Zn^{2+}$, thereby facilitating the $Zn^{2+}$ diffusion and de-solvation at low temperatures. Meanwhile, $Li^+$ can immobilize active $H_2O$ molecules and lower the freezing point of electrolyte, suppressing associated side reactions. Furthermore, a Li—Zn hybrid and F-rich SEI layer on the Zn metal surface can be formed during electrochemical cycling, ensuring high interface stability and rapid $Zn^{2+}$ migration through the SEI. Benefiting from this, the Zn metal anode can exhibit ultra-long cycling stability in symmetric cells (6500 h) at low temperature. And the full cells with NVO cathode can also demonstrate a high discharge capacity and cycling stability. Overall, this work offers a new design solution for gel electrolytes, enhancing the application prospects of ZIBs at low temperature.

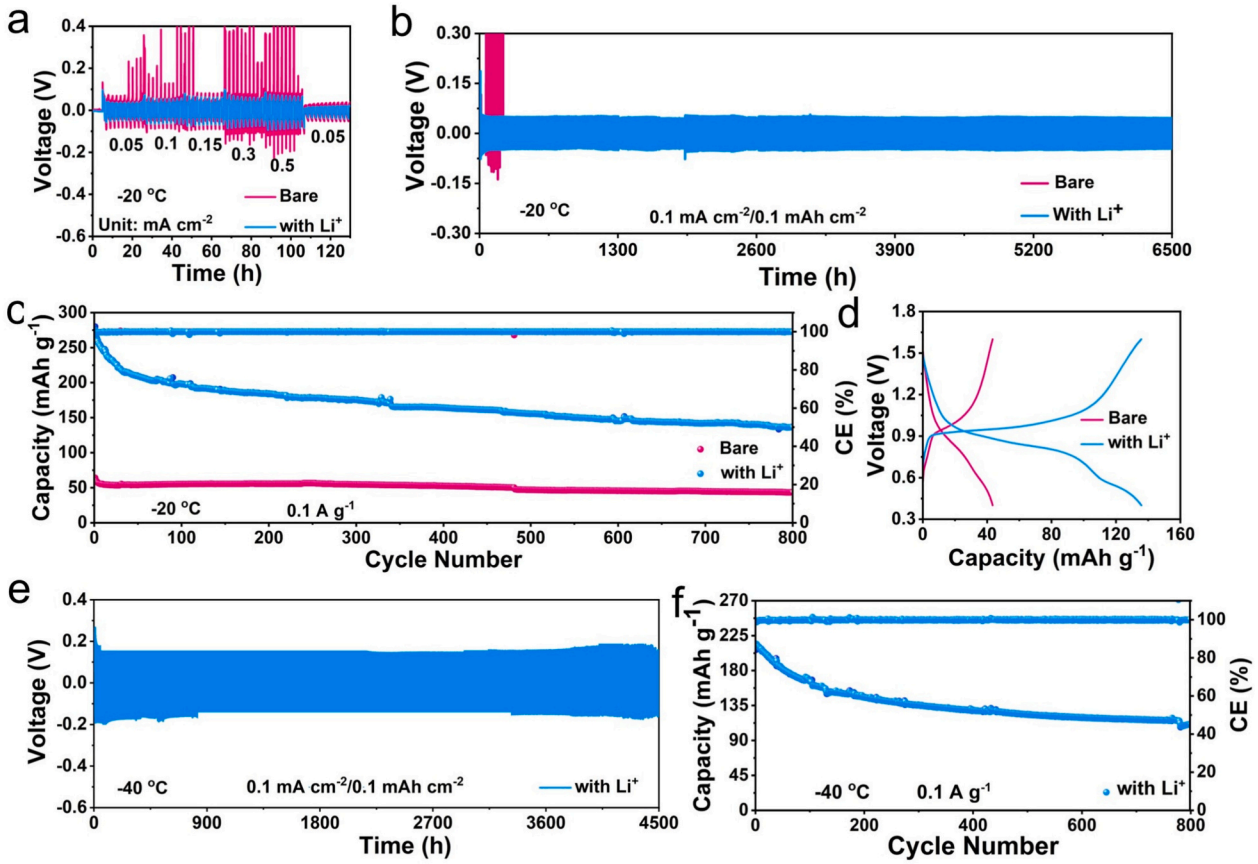


**Fig. 5.** Electrochemical performance at low temperature. a) Rate performance of symmetric cells at −20 °C; b) Long cycling stability of Zn || Zn symmetric cells at −20 °C; c) Cycling stability at −20 °C; d) Charge-discharge curves for 800 turns; e) Long cycling stability of Zn || Zn symmetric cells at −40 °C; f) Cycling stability of full cells at −40 °C.

## CRediT authorship contribution statement

**Mengfan Zhao:** Writing – original draft. **Bo Zhang:** Data curation. **Xiang Bai:** Funding acquisition. **Jiahui Zhang:** Funding acquisition. **Xinyue Chang:** Funding acquisition. **Lifeng Hou:** Writing – review & editing, Supervision. **Hao Huang:** Supervision, Data curation. **Shi Wang:** Writing – review & editing. **Zhong Jin:** Writing – review & editing. **Qian Wang:** Writing – review & editing, Supervision.

## Declaration of competing interest

The authors declare that they have no known competing financial interests or personal relationships that could have appeared to influence the work reported in this paper.

## Acknowledgements

This work was supported by the National Natural Science Foundation of China (No. 22402146), the Beijing Natural Science Foundation-Xiaomi innovation joint Foundation (L223011), Young Elite Scientists Sponsorship Program by CAST (2022QNRC001), Shanxi energy internet research institute (SXEI2023A004), Open Research Fund of Guangdong Advanced Carbon Materials Co., Ltd. (Kargen-2024B0905), the special fund for Science and Technology Innovation Teams of Shanxi Province (202204051001004).

## Appendix A. Supplementary data

Supplementary data to this article can be found online at https://doi.org/10.1016/j.cej.2025.166042.

## Data availability

Data will be made available on request.

## References

[1] X. Gong, J. Wang, Y. Shi, Q. Zhang, W. Liu, S. Wang, J. Tian, G. Wang, Inhibiting dendrites on Zn anode by ZIF-8 as solid electrolyte additive for aqueous zinc ion battery, Colloids Surf. A Physicochem. Eng. Asp. 656 (2023) 130255, https://doi.org/10.1016/j.colsurfa.2022.130255.

[2] Y. Li, Z. Wang, Y. Cai, M.E. Pam, Y. Yang, D. Zhang, Y. Wang, S. Huang, Designing advanced aqueous zinc-ion batteries: principles, strategies, and perspectives, Energy Environ. Mater. 5 (2022) 823–851, https://doi.org/10.1002/eem2.12265.

[3] H. Shi, S. Han, Z. Hou, H. Lan, S. Niu, Q. Li, Interactive issues and strategic solutions for aqueous Zn metal anodes, J. Energy Chem. 103 (2025) 163–187, https://doi.org/10.1016/j.jechem.2024.11.051.

[4] W. Zhang, Y. Dai, R. Chen, Z. Xu, J. Li, W. Zong, H. Li, Z. Li, Z. Zhang, J. Zhu, F. Guo, X. Gao, Z. Du, J. Chen, T. Wang, G. He, I.P. Parkin, Highly reversible zinc metal anode in a dilute aqueous electrolyte enabled by a pH buffer additive, Angew. Chem. Int. Ed. 62 (2023) e202212695, https://doi.org/10.1002/anie.202212695.

[5] H. Li, T. Feng, J. Gao, M. Wu, In situ construction of 3D crossing-linked gel polymer electrolyte toward high performance and safety lithium metal batteries, J. Power Sources 618 (2024) 235189, https://doi.org/10.1016/j.jpowsour.2024.235189.

[6] Y. Ren, X. Dong, Dynamic polymeric materials via hydrogen-bond cross-linking: effect of multiple network topologies, Prog. Polym. Sci. 158 (2024) 101890, https://doi.org/10.1016/j.progpolymsci.2024.101890.

[7] X. Yu, C. Liu, L. Wang, T. Li, L. Yuan, J. Yang, R. Xiao, Z. Wang, 3D printing of reprogrammable liquid crystal elastomers with exchangeable boronic ester bonds, Giant 20 (2024) 100331, https://doi.org/10.1016/j.giant.2024.100331.

[8] Y. Zhang, S. Shen, K. Xi, P. Li, Z. Kang, J. Zhao, D. Yin, Y. Su, H. Zhao, G. He, S. Ding, Suppressed dissolution of fluorine-rich SEI enables highly reversible zinc metal anode for stable aqueous zinc-ion batteries, Angew. Chem. Int. Ed. 63 (2024) e202407067, https://doi.org/10.1002/anie.202407067.

[9] L. Jia, H. Hu, X. Cheng, H. Dong, H. Li, Y. Zhang, H. Zhang, X. Zhao, C. Li, J. Zhang, H. Lin, J. Wang, Toward low-temperature zinc-ion batteries: strategy, progress, and prospect in vanadium-based cathodes, Adv. Energy Mater. 14 (2024) 2304010, https://doi.org/10.1002/aenm.202304010.

[10] X. Yang, Y. Zhao, S. Lv, L. Zhong, C. Yue, S. Zhan, L. Zhao, C. Wang, X. Li, X. Liu, Z. Tang, C. Zhang, C. Zhi, LvH.(Lyu), Anion-promoted CB[6] macromolecule dissolution for stable Zn-ion batteries, Energy Environ. Sci. 17 (2024) 4758–4769, https://doi.org/10.1039/D4EE01225A.

[11] H. Shi, S. Han, Z. Hou, H. Lan, S. Niu, Q. Li, Interactive issues and strategic solutions for aqueous Zn metal anodes, J. Energy Chem. 103 (2025) 163–187, https://doi.org/10.1016/j.jechem.2024.11.051.

[12] Q. Yang, L. Guo, Z. Liu, J. Wang, H. Luo, X. Zhang, Q. He, X. Chen, M. Li, Z. Wang, Y. Jiang, R. Yuan, Z. Liu, K. Zhang, Z. Hu, Y. Huang, Regulation of Zn2+ desolvation kinetics via interfacial hydrogen-bond network for a highly reversible Zn metal anode, Energ. Storage Mater. 75 (2025) 104028, https://doi.org/10.1016/j.ensm.2025.104028.

[13] S. Huang, S. He, S. Huang, X. Zeng, Y. Li, H. Noor, X. Hou, Molecular crowding agent modified polyanionic gel electrolyte for zinc ion batteries operating at 100 °C, Adv. Funct. Mater. (2024) 2419153, https://doi.org/10.1002/adfm.202419153.

[14] J. Kang, Z. Jiang, L. Wen, Directionally cast multilevel channels in hydrogel electrolyte for low-temperature aqueous zinc-ion batteries, Adv. Funct. Mater. (2025) 2422566, https://doi.org/10.1002/adfm.202422566.

[15] C.-C. Kao, J. Liu, C. Ye, S.-J. Zhang, J. Hao, S.-Z. Qiao, Building fast and selective Zn ion channels for highly stable quasi-solid-state Zn-ion batteries, J. Mater. Chem. A 11 (2023) 23881–23887, https://doi.org/10.1039/D3TA02866F.

[16] Y. Wang, Q. Li, H. Hong, S. Yang, R. Zhang, X. Wang, X. Jin, B. Xiong, S. Bai, C. Zhi, Lean-water hydrogel electrolyte for zinc ion batteries, Nat. Commun. 14 (2023) 3890, https://doi.org/10.1038/s41467-023-39634-8.

[17] S.Y. Fan, X.L. Xu, W.J. Wu, High-temperature-operating (over 140 °C) Li-ion supercapacitor via water-locking bimodal cross-linked hydrogel, Mater. Today Chem. 30 (2023) 101549, https://doi.org/10.1016/j.mtchem.2023.101549.

[18] H. Peng, D. Wang, F. Zhang, L. Yang, X. Jiang, K. Zhang, Z. Qian, J. Yang, Improvements and challenges of hydrogel polymer electrolytes for advanced zinc anodes in aqueous zinc-ion batteries, ACS Nano 18 (2024) 21779–21803, https://doi.org/10.1021/acsnano.4c06502.

[19] G. Liu, S. Zhang, Y. Peng, M. Yu, L. Zhao, J. Zhang, Y. Meng, F. Ran, Improving diffusion kinetics of zinc ions/stabilizing zinc anode by molecular slip mechanism and anchoring effect in supramolecular zwitterionic hydrogels, J. Colloid Interface Sci. 678 (2025) 159–167, https://doi.org/10.1016/j.jcis.2024.09.128.

[20] H. Peng, D. Wang, F. Zhang, L. Yang, X. Jiang, K. Zhang, Z. Qian, J. Yang, Improvements and challenges of hydrogel polymer electrolytes for advanced zinc anodes in aqueous zinc-ion batteries, ACS Nano 18 (2024) 21779–21803, https://doi.org/10.1021/acsnano.4c06502.

[21] T. Lu, Y. Lin, L. Guan, L. Hou, H. Du, H. Wei, X. Liu, C. Yang, Y. Wei, M. Song, W. Liu, H. Zhou, Q. Wang, Suppressing side reaction and dendritic growth via interfacial cyclization molecule for stable Zn metal anodes, ACS Appl. Energ. Mater. 7 (2024) 61–71, https://doi.org/10.1021/acsaem.3c02209.

[22] W. Yu, Z. Yu, Y. Cui, Z. Bao, Degradation and speciation of Li salts during XPS analysis for battery research, ACS Energy Lett. 7 (2022) 3270–3275, https://doi.org/10.1021/acsenergylett.2c01587.

[23] Q. Zhang, Y. Ma, Y. Lu, L. Li, F. Wan, K. Zhang, J. Chen, Modulating electrolyte structure for ultralow temperature aqueous zinc batteries, Nat. Commun. 11 (2020) 4463, https://doi.org/10.1038/s41467-020-18284-0.

[24] T. Wei, Y. Ren, Z. Li, X. Zhang, D. Ji, L. Hu, Bonding interaction regulation in hydrogel electrolyte enable dendrite-free aqueous zinc-ion batteries from −20 to 60 °C, Chem. Eng. J. 434 (2022) 134646, https://doi.org/10.1016/j.cej.2022.134646.

[25] Y. Ye, Y. Zhang, Y. Chen, X. Han, F. Jiang, Cellulose nanofibrils enhanced, strong, stretchable, freezing-tolerant ionic conductive organohydrogel for multi-functional sensors, Adv. Funct. Mater. 30 (2020) 2003430, https://doi.org/10.1002/adfm.202003430.

[26] S. Huang, L. Hou, T. Li, Y. Jiao, P. Wu, Antifreezing hydrogel electrolyte with ternary hydrogen bonding for high-performance zinc-ion batteries, Adv. Mater. 34 (2022) 2110140, https://doi.org/10.1002/adma.202110140.

[27] C. Liu, B. Zhang, Z. Liang, X. Bai, J. Zhang, X. Chang, L. Hou, H. Huang, Y. Wei, B. Wu, S. Wang, C. Yang, W. Liu, Q. Wang, Synergistically modulating the inner Helmholtz plane and outer Helmholtz plane to achieve a stable interface for aqueous zinc ion batteries, Chem. Eng. J. 508 (2025) 160900, https://doi.org/10.1016/j.cej.2025.160900.

[28] R. Fu, B. Zhang, T. Lu, C. Liu, L. Hou, S. Wang, Y. Ning, Z. Jin, Q. Wang, A dilute and non-flammable electrolyte engineering enables stable SEI for low-temperature zinc batteries, Energ. Storage Mater. 80 (2025) 104374, https://doi.org/10.1016/j.ensm.2025.104374.

[29] B. Wu, T. Lu, X. Bai, J. Zhang, X. Chang, L. Hou, Y. Wei, Q. Wang, J. Ni, Dual-induced directed deposition mechanism based on anionic surfactants enables long cycle aqueous zinc ion batteries, Small Methods (2025) 2401838, https://doi.org/10.1002/smtd.202401838.

[30] R. Chen, W. Zhang, C. Guan, Y. Zhou, I. Gilmore, H. Tang, Z. Zhang, H. Dong, Y. Dai, Z. Du, X. Gao, W. Zong, Y. Xu, P. Jiang, J. Liu, F. Zhao, J. Li, X. Wang, G. He, Rational design of an *in-situ* polymer-inorganic hybrid solid electrolyte interphase for realising stable Zn metal anode under harsh conditions, Angew. Chem. Int. Ed. 63 (2024) e202401987, https://doi.org/10.1002/anie.202401987.

[31] B. Li, B. Zhang, X. Bai, J. Zhang, X. Chang, L. Hou, H. Huang, T. Lu, S. Wang, Z. Jin, Q. Wang, A dynamic self-healing protective layer enabling stable zinc ion batteries through strong Zn-S affinity and intramolecular hydrogen bonding, Angew. Chem. Int. Ed. (2025) e202503345, https://doi.org/10.1002/anie.202503345.

[32] F. Hu, Y. Gu, F. Cui, G. Song, K. Zhu, High-performance (NH4)2V6O16·0.9H2O nanobelts modified with reduced graphene oxide for aqueous zinc ion batteries, Chin. Chem. Lett. 32 (2021) 3793–3798, https://doi.org/10.1016/j.cclet.2021.04.032.

[33] S. Cui, W. Miao, X. Wang, K. Sun, H. Peng, G. Ma, Multifunctional zincophilic hydrogel electrolyte with abundant hydrogen bonds for zinc-ion capacitors and

supercapacitors, ACS Nano 18 (2024) 12355–12366, https://doi.org/10.1021/acsnano.4c01304.

[34] Y. Liu, L. Zhang, L. Liu, Q. Ma, R. Wang, P. Xiong, H. Li, S. Zhang, J. Hao, C. Zhang, All-climate energy-dense cascade aqueous Zn-$I_2$ batteries enabled by a polycationic hydrogel electrolyte, Adv. Mater. (2025) 2415979, https://doi.org/10.1002/adma.202415979.

[35] S.-J. Guo, M.-Y. Yan, D.-M. Xu, P. He, K.-J. Yan, J.-X. Zhu, Y.-K. Yu, Z.-Y. Peng, Y.-Z. Luo, F.-F. Cao, Anti-freezing hydrogel electrolyte with a regulated hydrogen bond network enables high-rate and long cycling zinc batteries, Energy Environ. Sci. 18 (2025) 418–429, https://doi.org/10.1039/D4EE02772H.